eprints@whiterose.ac.uk
https://eprints.whiterose.ac.uk/

SYSTEMATIC VARIATIONS OF MACROSPICULE PROPERTIES OBSERVED BY *SDO*/AIA OVER HALF A DECADE

T. S. Kiss[1,2], N. Gyenge[1,3], and R. Erdélyi[1]

[1] Solar Physics and Space Plasmas Research Centre (SP2RC), School of Mathematics and Statistics, University of Sheffield Hicks Building, Hounsfield Road, Sheffield, S3 7RH, UK; robertus@sheffield.ac.uk
[2] Department of Physics, University of Debrecen, Egyetem tér 1, Debrecen, H-4010, Hungary
[3] Debrecen Heliophysical Observatory (DHO), Research Centre for Astronomy and Earth Sciences, Hungarian Academy of Sciences Debrecen, P.O.Box 30, H-4010, Hungary

ABSTRACT

Macrospicules (MSs) are localized small-scale jet-like phenomena in the solar atmosphere, which have the potential to transport a considerable amount of momentum and energy from the lower solar atmospheric regions to the transition region and the low corona. A detailed statistical analysis of their temporal behavior and spatial properties is carried out in this work. Using state-of-the-art spatial and temporal resolution observations, yielded by the Atmospheric Imaging Assembly of *Solar Dynamics Observatory*, we constructed a database covering a 5.5 year long period, containing 301 macrospicules that occurred between 2010 June and 2015 December, detected at 30.4 nm wavelength. Here, we report the long-term variation of the height, length, average speed, and width of MS in coronal holes and Quiet Sun areas both in the northern and southern hemisphere of the Sun. This new database helps to refine our knowledge about the physical properties of MSs. Cross-correlation of these properties shows a relatively strong correlation, but not always a dominant one. However, a more detailed analysis indicates a wave-like signature in the behavior of MS properties in time. The periods of these long-term oscillatory behaviors are just under two years. Also, in terms of solar north/south hemispheres, a strong asymmetry was found in the spatial distribution of MS properties, which may be accounted for by the solar dynamo. This latter feature may then indicate a strong and rather intrinsic link between global internal and local atmospheric phenomena in the Sun.

Key words: Sun: chromosphere – Sun: corona – Sun: activity – Sun: oscillations

1. INTRODUCTION

Our knowledge of the different layers and structures of the solar atmosphere has improved greatly in the past decades. However, the structural fine-scale details of the atmosphere still leave many open questions (see the review papers of e.g., Judge 2006; Lipartito et al. 2014). A challenging task is to identify and catalog the small-scale, localized observable phenomena (e.g., bushes, fibrils, flocculi, grains, mottles, spicules, etc.) present in the chromospheric zoo in regards of their numbers and variety. These often rapidly appearing and disappearing, fine structures are popularly observed in, e.g., the He II (≈30.4 nm) emission line, Hα (≈656.28 nm), and Ca II (≈393.366 nm) absorption lines.

One class of the set of highly dynamic phenomena is the spicules. They are abundant, spiky-like gas jets at the chromospheric solar limb (Secchi 1877). Their upward mass flux is about 100 times that of the solar wind (Sterling 2000; de Pontieu et al. 2004; Sterling et al. 2010). Spicules are detectable both on the disk (often called as mottles) and at the limb at any given moment of time. Depending on their size and lifetime, spicules can be classed into two groups. Spicules with 7000–11,000 km length, 5–15 minute lifetime, and 25 km s^{-1} propagating speed are called "classic," or lately debatably referred to as type-I spicules (Beckers 1968; Zaqarashvili & Erdélyi 2009). The other group is claimed to contain the smaller and faster (5000 km average height, 50–100 km s^{-1} propagation speed) so-called type-II spicules (on disk often labeled as Rapid Blueshifted Excursiors (RBEs) referring to one of their distinct observable properties) with shorter lifetime, 10–150 s (de Pontieu et al. 2007, 2012; Sekse et al. 2012; Kuridze et al. 2015). Spicules, irrespective of their lifetime and

speed, could play an important role in the energy and momentum transportation from the photosphere to the chromosphere or low corona. Their capability of guiding MHD waves is discussed by, e.g., Zaqarashvili & Erdélyi (2009).

There are, however, much larger spicule-like, also abundant, dynamic jets detected to be present in the solar atmosphere: macrospicules (MSs). The investigation of macrospicules reaches back at least 40 years. The first modern observation of macrospicules was carried out by Bohlin et al. (1975). With the 30.4 nm spectroheliograph onboard the *Skylab* mission, Bohlin et al. (1975) identified 25 MSs with lengths of 8″–25″ (some extreme cases were even with 30″–60″). Their lifetime is about 8–45 minutes without any reported correlation at that time between the length and lifetime. Most MSs are formed inside coronal hole (CH) regions. Their name, initially, was suggested to be "EUV macrospiclues" after the wavelength band they were detected in.

Labonte (1979) observed 32 macrospicules with the 25 cm aperture vacuum telescope at Big Bear Solar Observatory using Hα and D$_3$ filters during an observation campaign of 122 hr. The length (8″–33″) and lifetime (4–24 minute) of these MSs were similar to those reported in Bohlin et al. (1975). Dere et al. (1989) investigated 10 MSs with the UV spectroheliograph onboard the *Spacelab-2* mission. The properties of the MSs found were similar, again, to those reported in the previous two studies, but the main innovation is the development of temporal resolution: *Spacelab-2* was able to observe macrospicules with a lifetime down to three minutes.

The breakthrough came with the age of high-resolution spacecraft: *Solar Heliospheric Observatory* (*SOHO*, Fleck et al. 2000) opened new avenues in solar physics with much greater temporal and spatial resolution than before. In the
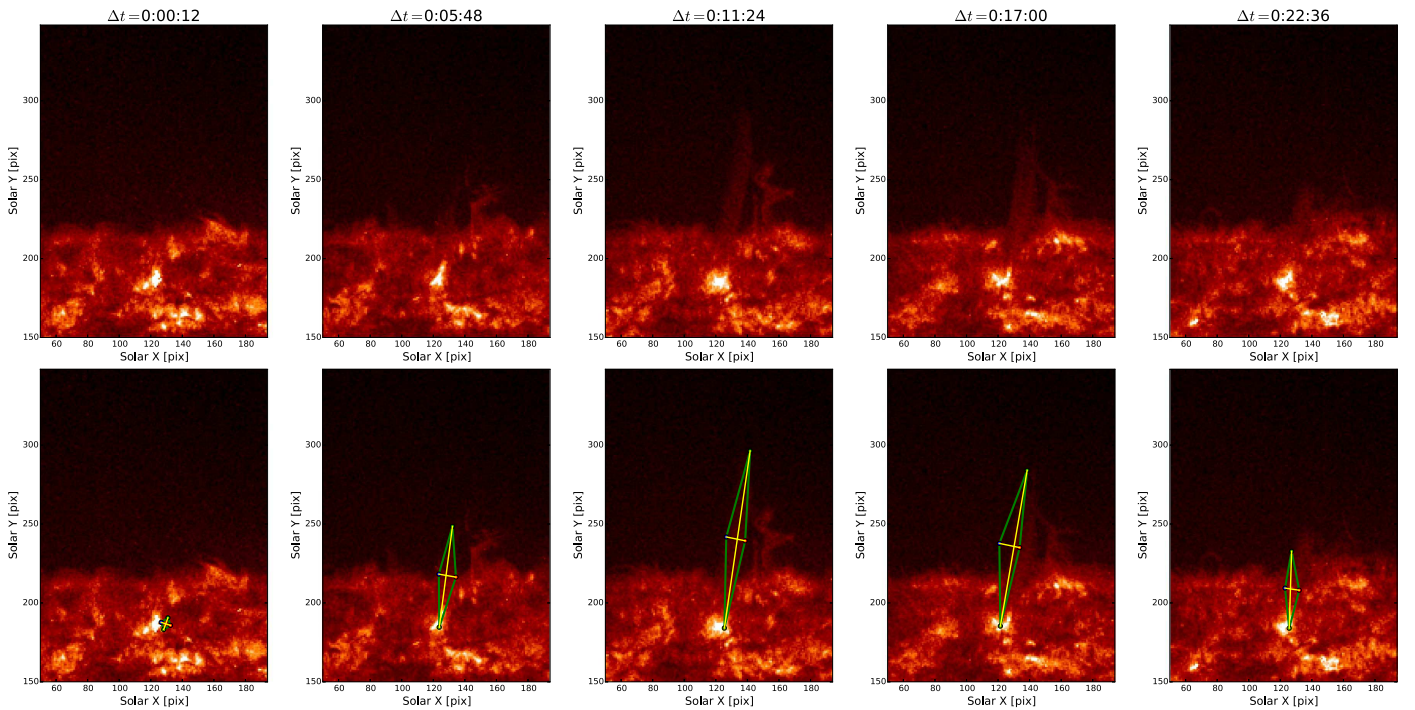
Figure 1. Series of images about a Quiet Sun macrospicule on *SDO*/AIA 30.4 nm images. The phenomenon occurred between 12:20 and 12:43 on 03.07.2012 on the western solar limb. The bottom panel images are overplotted by the tetragon assumption of MS. In the first column, the brightening is clearly visible, which may be the precursor of the jet itself.

context relevant for our paper, we recall that Pike & Harrison (1997) used *SOHO*/Coronal Diagnostic Spectrometer (CDS) to investigate the physics of MSs with the first multi-wavelength observation and described them as multi-thermal structures. The authors claimed that X-ray jets and EUV MSs are a manifestation of the same underlying physical phenomena, which could be the source of the fast solar wind as well. They also described, first, an associated "pre-existing bright point," which can be a sub-flare brightening.

In a follow-up study, Pike & Mason (1998) employed *SOHO*/CDS to detect the rotational properties of MSs. Blue and redshifted emission was observed on either side of the axis of MSs above the limb, which suggests the rotation of MSs. The rotation velocities increase with height, so the macrospicules they observed were labeled "solar tornadoes." The separation of blue- and redshifted regions on two sides of the macrospicule is clearly visible.

Parenti et al. (2002) investigated the density and temperature of MSs. Three data sets, taken by *SOHO*/CDS and *SOHO*/Normal Incidence Spectrometer (NIS), were constructed. The first data set contains information about the MSs, while the two others are averaged and used as a "background" to reduce the noise of the first one. The subtraced spectra showed a number of new properties: MS density was about 10^{-10} cm^{-3} while the temperature was $3–4 \times 10^5$ K. The employed noise-reduction technique gave an opportunity to investigate the motion and the trajectory of MSs: a maximum velocity was found to be about 80 km s^{-1} during the entire lifetime. The maximum height reached by MSs was reported to be 6×10^4 km above the solar limb. The average speed of falling back was about 26 km s^{-1}.

Scullion et al. (2010) examined both on-limb and off-limb MSs with the high-resolution spectroscopic capability of *SOHO*/Solar Ultraviolet Measurements from Emitted Radiation (SUMER) instrument. In the case of two off-limb events,

fast upward propagation was measured between the mid-transition region (N VII—765 Å) and the lower corona (Ne VIII—770 Å) with ≈ 145 km s^{-1}. On-limb observations suggest that spicules can be precursors for macrospicules.

Madjarska et al. (2011) analyzed three macrospicules with four instruments (*Hinode*/SOT, EIS, XRT and *SOHO*/SUMER). These co-aligned images revealed that macrospicules do not seem to appear in a spectral line formed over 300,000 K.

On the theoretical side, Murawski et al. (2011) carried out one of the first numerical simulations for MSs as a velocity-shock in the transition region. They employed the FLASH code (Lee & Deane 2009) to solve the two-dimensional MHD equations by implementing a VAL IIIC solar temperature model (Vernazza et al. 1981). Many properties of simulated MSs matched the abovementioned, observed lifetime, length, and velocity.

Another new era of MS observation has began with the launch of *Solar Dynamics Observatory* (*SDO*) in 2010 (Pesnell et al. 2012). Onboard the spacecraft, the Atmospheric Imaging Assembly (*SDO*/AIA) generates terabytes of full-disk data with 0″.6 spatial and 12 s temporal resolution at e.g., 30.4 nm wavelength (Lemen et al. 2012).

Kayshap et al. (2013) carried out a detailed description of the evolution of an individual MS. This jet occurred in the north polar corona on 2010 November 11 with nearly 24 minutes lifetime and 40 Mm height. Based on its detailed observational description, a two-dimensional numerical simulation was performed using the VAL IIIC initial atmospheric model (Vernazza et al. 1981). A small-scale magnetic flux tube emerged from the sub-photospheric layers into the previously existing open magnetic field, then underwent kink-oscillation. The authors claimed that this kinking motion is the source of the MS. The flux-emerging model is one of the widely accepted

Figure 2. Distributions, from top to bottom: maximum area, maximum length, lifetime, average velocity and maximum width. In each panel, on the LHS, the distribution of the actual property can see. Different types of mark are used for different hemispheres: diamonds represent the northern hemisphere (dark blue—CH, light blue—QS), circles denote the south (green—CH, red—QS). On the right-hand panels, the histogram of each distributions is provided. The dashed line indicates the fitted log-normal distributions. The vertical line represents the mode of the distribution (light-darker-dark strips correspond to 1σ, 2σ, 3σ distributions).

theories of solar jets (for a review of this topic, see Sterling 2000).

According to the study by Gyenge et al. (2015), using *SDO*/AIA data, the spatial distribution of macrospicules shows inhomogeneous but systematic properties. It is known that the latitudinal distribution of MSs concentrates around the poles. However, from the study of Gyenge et al. (2015) the longitudinal distribution also shows inhomogeneous properties. The longitudinal positions tend to focus around certain belts, which suggests that there is a relationship between the position occurrence and the generation of the global magnetic field.

Taking advantage of the uninterrupted observations of *SDO*, Bennett & Erdélyi (2015) built up a data set with 101 MSs covering an observation over a 2.5 year long time interval. The authors claim that features like maximum length (28 Mm), upflowing velocity (110 km s^{-1}) and lifetime (14 minute) are varying in time systematically. Cross-correlation of maximum length–maximum velocity and lifetime–maximum length showed a significant correlation ($k = 0.43, 0.66$), however the correlation coefficient is much smaller in the case of maximum velocity and lifetime ($k = 0.16$). Ballistics of MSs were investigated as well, which indicates a strong influence of gravity in the rise and fall of MSs. Taking stock of the ballistics and two characteristic density values of MSs ($\rho = 1.0 \times 10^8$ kg m^3 and $\rho = 1.0 \times 10^{11}$ kg m^3), the authors estimated the formation energy 1.46×10^{17} J, 4.78×10^{16} J, 3.09×10^{15} J, 1.46×10^{14} J for 25, 5, 1, and 0.5 Mm scale heights and 3.66×10^{13} J for uniform plasma distribution cases.

In this study, we focus on the statistical investigation of the temporal behavior of MSs on timescales spanning considerably longer than previous studies, i.e., for a time interval of just under 6 years. This extended temporal investigation yields the opportunity to analyze the temporal variation of MS properties and the detection of the oscillatory behavior of their properties on roughly biannual timescales, well beyond the lifetime of individual MSs. In Section 2, we introduce the way the database was built up. In Section 3, we discuss the results of the statistical analysis. We outline our discussion and conclusions in the last section.

2. DATABASE

The source and driving force of the majority of solar phenomena is the large-scale, global magnetic field, which varies on a long-term, e.g., 11 year time, period. However, the temporal behavior of jets is always considered on a short timescale. That may be the reason why previous studies have investigated only a few MSs over a short time period. The temporal ranges of jet evolution are much shorter than the characteristic timescale of the solar cycle. Therefore, investigation of the properties of short-timescale macrospicules over a long time period is still an uncharted territory with some interesting questions to answer. To achieve this objective, an instrument is required (i) to have high temporal and spatial resolution to properly resolving the jets themselves, and (ii) to operate continuously for multiple years in order to investigate long-term evolution in a statistical sense. The ideal choice is *SDO*, which was launched in 2010 June, near to solar minimum between solar cycles 23 and 24. The operation of *SDO* for a period of about 6 years, at the time of writing, provides a great opportunity to acquire the long-term temporal variation of the properties of MSs in the current solar cycle.

SDO/AIA 30.4 nm images may be divided into three regions due their overall average intensity. Active regions (ARs) are bright, fine-detailed areas often near the solar equator; at the same time CHs are mostly formed around the solar poles and their reduced intensity is related to the open magnetic field (Aschwanden 2004). Finally, the Quiet Sun area (QS) is defined as non-AR or non-CH solar surface. Therefore, the macrospicules we studied were named and cataloged as coronal hole (CH–MSs) and Quiet Sun (QS–MSs) macrospicules, distinguished by the surrounding solar environment. We have not investigated AR MSs; for reasoning see below.

To build a long-term database with a sufficient number of observations for statistical analysis, a strict definition of what is actually considered a MS is necessary. Let us summarize how we define a MS by the following five points. First, MSs are "thin" jet phenomena at the solar limb. Second, MSs generated in ARs are not selected, just those from CH and Quiet Sun areas. The reason for this apparently perhaps too-restrictive criterion is that the large-scale magnetic field of ARs is able to drive MS-like phenomena (Chandra et al. 2015; Sterling et al. 2016), which could be different in terms of physics from MSs formed in CH or QS areas (Kayshap et al. 2013). Third, MSs are shorter than 200 pixels (70 Mm). This, perhaps somewhat arbitrary, upper limit avoids contaminating our data set with other high-energetic jet phenomena. Fourth, MSs have to have a visible connection with the solar surface. The lack of connection may mean that the MS is formed on the "other side," i.e., far side, of the solar limb. If far-side MSs were considered, this may carry an error to the estimate of the distance between the top and the footpoint of MS. Fifth, and perhaps most distinctly, 1–2 minutes before the appearance of the MS jet, a brightening is identifiable at the solar surface. The presence of brightening actually also confirms that the MS is on the visible side of the Sun. A number of previous works discussed the physics of brightening generation (Pike & Harrison 1997; Sterling et al. 2015).

To provide a temporally homogeneous data set, MSs were identified and chosen from a 2 hr long interval between 12:00 and 14:00 on every 1st, 7th, 15th, 24th day of each month from 2010 January 06 until 2015 December 31.

To turn macrospicules identified by *SDO* observations to geometrically, e.g., morphologically, measurable features, MSs were fitted with tetragons (see Figure 1). Note, we are not saying MSs have a tetragonal shape. On the contrary, MSs have an irregular shape. Figure 1 shows a complete evolution of a QS-MS on the western limb in five images with ∼5.5 minutes temporal differences. We only approximate their geometric extent in order to estimate their length, width, etc. A framework of Sunpy (see e.g., Mumford et al. 2013) was used for this process. On every tetragon, two of the diagonal points represent the bottom and top, and the distance between them measures the actual length of the jet. The distance between the remaining two points models the width of the MS perpendicular to the main axis. Furthermore, the position of bottom point of the MS was assigned with the actual observing time. Data about a MS contain the position of four vertices for every frame of observation, where the MS is clearly visible.

By applying the above outlined criteria to *SDO*/AIA 30.4 nm observation, 301 MSs have been detected during 5.5 years of sequence of observation. The number of different types of macrospicule are not equal in terms of location: 158 jets formed (≈52.48% of all MS) in CHs and only 134 took
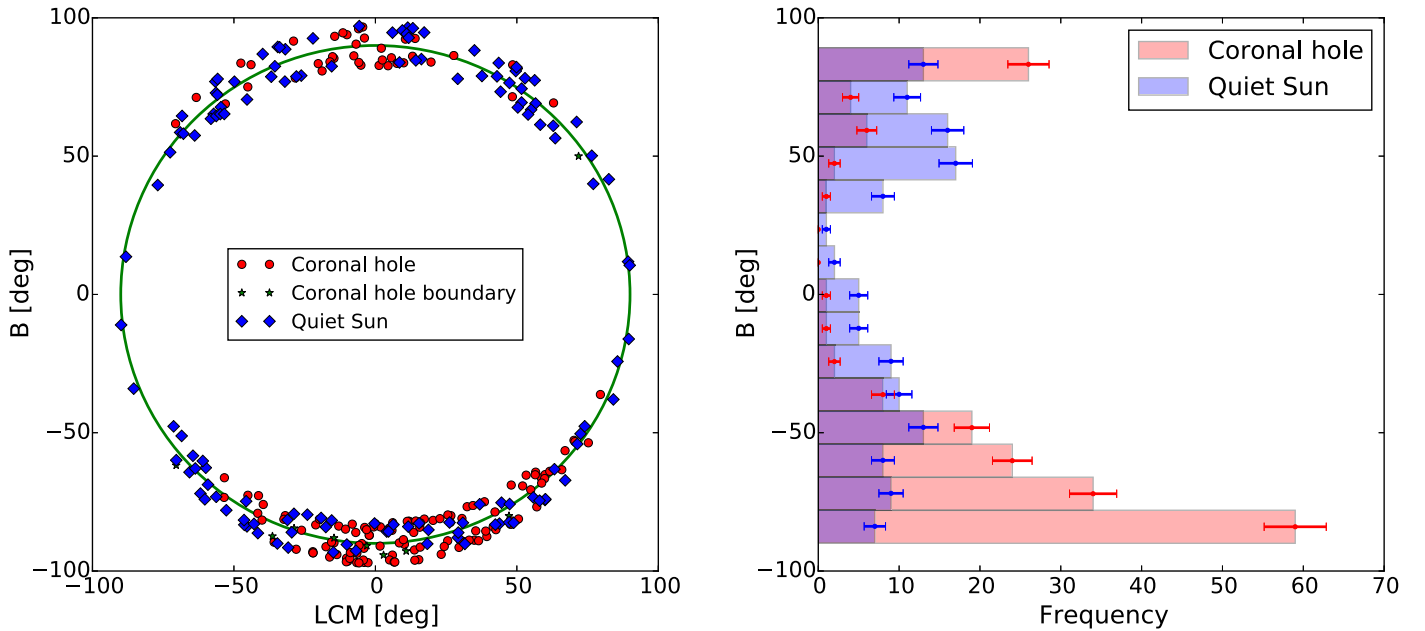
Figure 3. On the left-hand side locations of all investigated MSs are plotted around the solar limb. Red, blue and green mark the coronal hole, Quiet Sun and coronal boundary MSs, respectively. The vertical axis is the heliographic latitude (B). Longitude of central meridian (LCM) is along the horizontal axis. On the right-hand side, a histogram of CH–MS and QS–MS location is provided with red and blue strips, respectively.

place (≈44.50% of all MS) in Quiet Sun regions. Occasionally a MS was not registered into this dual system, therefore a new class, named coronal hole boundary (CHB), was assigned to catalog them. However the number of CHB macrospicules is only 9 (≈0.02% of all MS). For this reason, we have not applied the same statistical studies to CHB MS that we have in the cases of CH or QS macrospicules.

On-disk MSs are often associated with explosive phenomena. These events (therefore MSs as well) are regions of excess line width, which were observed recently to a greater extent in CHs than Quiet Sun regions (Kayshap et al. 2015).

3. RESULTS

3.1. Spatial Distribution on the Solar Disk

For each frame during the entire lifetime of a MS, the position of the four edges of their tetragon is built up from two polar coordinates: the first represents the distance from the solar disk center, the second one shows a polar degree from along the solar limb. From these two data values the actual position of a MS on the solar disk is easily determinable. Because each tetragon was fitted individually at different time frames, the position of the associated MS varies on a small, approximately 3 arcsec distance. This variation is neglectable, so in this study, the position of the MS is always denoted with the position of the brightening observed on the first frame.

By estimating the positions of all the observed MSs in our database, it is clearly visible that MSs are formed mostly around the solar poles. There may be a bias caused by the introduced selection criteria, namely we exclude ARs that are more abundant around the solar equator. Furthermore, the ratio between the number of CH–MSs and QS–MSs could be influenced by the solar dynamo: when the poloidal field is more dominant (e.g., during solar minima), the area of CH regions may be larger. Therefore the number of CH–MSs could grow substantially. This effect may be reversed during solar maxima with less dominant poloidal fields. The histogram of the spatial

distribution shows what is expected: CH–MSs mostly take place around the solar poles, while QS–MSs cuddle around them as a "ring" as seen in the right-hand side of Figure 3.

Another interesting aspect is the ratio between the number of MSs on the two solar hemispheres. For QS–MSs, the corresponding numbers are nearly equal ($n_{North\_QS} = 69$, $n_{South\_QS} = 65$), but a huge difference is found between the northern and southern CH–MSs numbers ($n_{North\_CH} = 39$, $n_{South\_CH} = 119$).

Strong asymmetry between the two hemispheres is visible in the heliospheric current sheet position, therefore the inclination of polar jets (Nisticó et al. 2015). For the period of 2007–2008 solar minima, the authors found that jets are deflected towards low latitudes and this deflection is more pronounced at the north pole than at the south pole. Asymmetry was also reported in many different magnetic solar phenomena: e.g., sunspots (Chowdhury et al. 2013; Kitchatinov & Khlystova 2014), global distribution of the solar wind speed (Hoeksema 1995) and magnetic field measurements in the interplanetary medium (Erdős & Balogh 2010). These results suggest an influencing effect by the solar dynamo (Shetye et al. 2015).

3.2. Measuring Macrospicule Properties

Many different properties of MSs, such as length, lifetime, width, area, and rise (i.e., emergence) velocity, have been refined in several studies in the last 40 years. Therefore a crucial cross-checking point of this study now is how well our results fit with those reported by others. The tetragon assumption is a powerful tool to determine key properties in the following ways: (a) maximum length is the greatest distance between the bottom and the top points; (b) maximum width represents the greatest distance between the two side diagonal points; (c) average upflow velocity is the average of speed values calculated from spatial difference between two frames in the emerging epoch of MS life; (d) lifetime is the temporal difference between the first and last frame where the

Table 1
Preferences of the Fitted Log-normal Distributions

	Mode	Mean	Median	Distribution		
				1σ	2σ	3σ
Maximum length [Mm]	24.95	28.07	26.99	20.39–35.72	15.41–47.27	11.64–62.56
Maximum lifetime [s]	916.72	1015.88	981.69	755.68–1275.3	581.70–1656.73	447.77–2152.24
Maximum width [″]	3.95	4.98	4.61	3.11–6.83	2.10–10.12	1.42–14.99
Average velocity [km s^{-1}]	59.62	73.25	68.39	47.22–99.05	32.60–143.46	22.51–207.77
Maximum area [Mm^2]	69.01	97.787	87.06	53.77–140.97	33.2–228.26	20.5–369.61

Note. 1σ distribution covers 68%, 2σ represents 95%, 3σ marks 99.5% of data.

Table 2
Summary of Macrospicules Based on Previous Studies

	Bohlin et al. (1975)	Labonte (1979)	Dere et al. (1989)	Bennett & Erdélyi (2015)	New Results (1σ)
Length [Mm]	6.24–19.45	6.24–25.67	3.9–17.9	14–68.46	20.39–35.72
Lifetime [minute]	8–45	4–24	⩾3	2.7–30.6	12.5–21
Velocity [km s^{-1}]	10–150	⩽60	20–50	54.1–335.5	47.22–99.05
Width [Mm]	3.6–10.9	2.2–6.5	…	3.1–16.1	2.1–10.1
Spectral line	He II (λ304)	Hα (λ6562)	C IV (λ1548)	He II (λ304)	He II (λ304)
log temperature of line [K]	4.9	4.0	5.0	4.0	4.0
Number of MS	~25	32	10	101	301
Spatial resolution [″]	2	0.5	2	1.5	1.5
Temporal resolution [s]	⩾180	~60	20, 60	12	12

MS is visible, and (e) maximum area shows the maximal value of geometrical areas of all tetragons during the whole lifetime of a MS.

As a first approximation, determining these values for each MS and plotting them in time, no obvious temporal variation is found. To have a more accurate understanding of the range of characteristic values determining MS properties, their histogram was investigated. A log-normal distribution is fitted to each histogram as seen in Figure 2. The main properties of each fit (e.g., mode, median, mean, scattering, distribution) to the data are in Table 1. These obtained values are found to be in line with those reported previously in the literature. In particular, three properties show great similarity: lifetime (16.75 ± 4.5 minutes), maximum width (6.1 ± 4 Mm), and average upflow velocity (73.14 ± 25.92 km s^{-1}). The maximum length is nearly overestimated here, with 28.05 ± 7.67 Mm. These similarities indicate a positive feedback to the criteria that we have set for defining MSs, and the applicability of tetragon assumption as well. For a summary of the comparison of average properties found here with those reported in earlier studies, see Table 2.
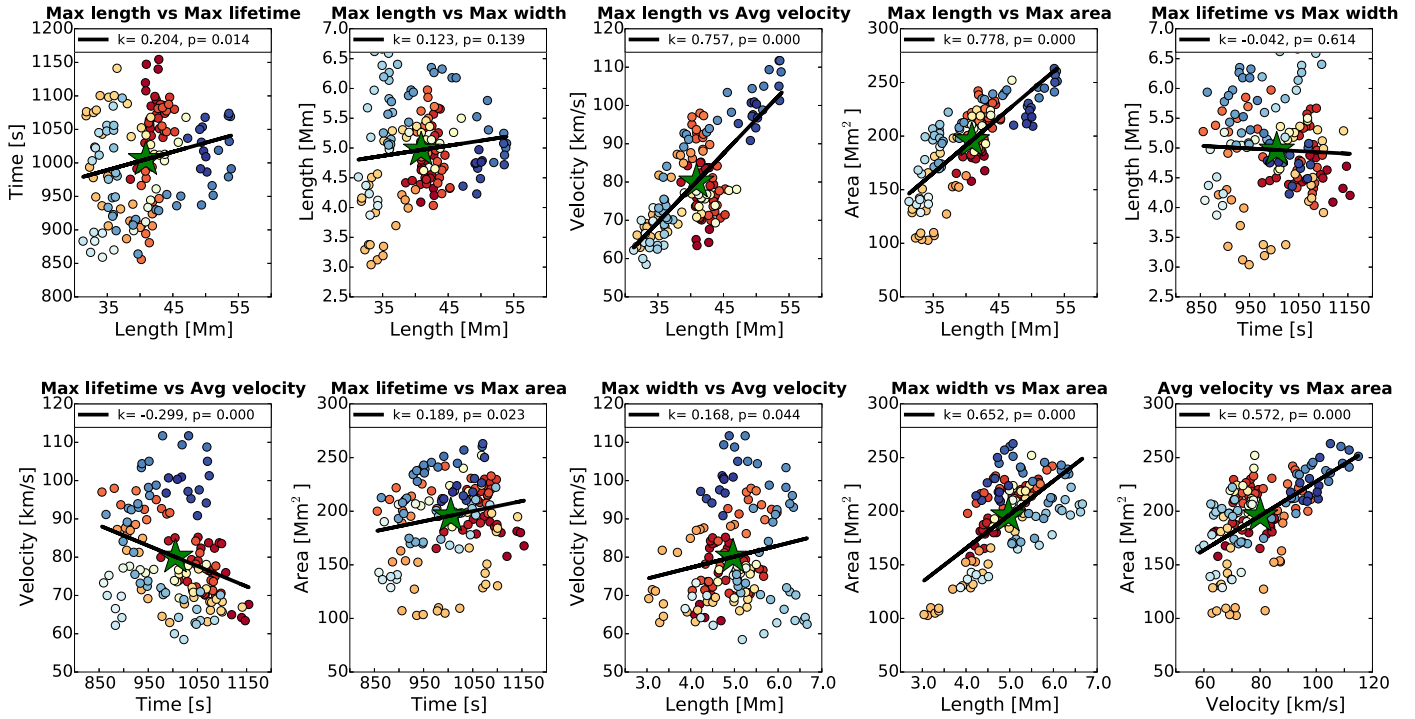
3.3. Cross-correlation of Properties

In the next step, we aim to discover whether there is any correlation between the properties of MSs found. For this reason, selected properties are plotted against each other. To show whether any two properties correlate, a linear fitting is applied to the data distribution. This fit is displayed in Figure 4. The correlation coefficients (k) were also determined, and it seems to have a relatively small value for both CH ($k_{CH} = [-0.29, -0.012, 0.127, 0.131, 0.195, 0.214, 0.557]$) and QS ($k_{QS} = [0.179, 0.355, 0.373, 0.406, 0.58]$) type MSs. This suggests that there is no strong correlation between the different properties of MSs in general. In both cases, only a small number of combinations show stronger correlations. "Maximum

length versus maximum area" ($k_{CH} = 0.78$, $k_{QS} = 0.87$), "maximum width versus maximum area" ($k_{CH} = 0.64$, $k_{QS} = 0.75$) and "maximum length versus average velocity" ($k_{CH} = 0.76$, $k_{QS} = 0.81$) seem to have relatively strong correlations for both CH–MSs and QS–MSs. A correlation between data sets cannot be negligible if the correlation coefficient is greater than around 0.6. In this respect the above stronger correlations seem to be logical, as area data are derived from the length and width. Further, "maximum area versus average velocity" ($k_{QS} = 0.71$) and "maximum area versus maximum lifetime" ($k_{QS} = 0.65$) pairs indicate a stronger correlation for QS–MSs only.

Next, there is a visible gap between CH–MSs and QS–MSs in their average correlation coefficient ($|k_{CH\_avg}| = 0.372$, $|k_{QS\_avg}| = 0.57$) and the ratio of the correlation coefficient is also greater than 0.6 ($n_{k\_CH} = 3/10$, $n_{k\_CH} = 5/10$). The source of these differences may be rooted in the underlying, governing physical differences between the two types of MS, which should be clarified in future research but is not within the scope of the present paper.

By investigating the large-scale time-dependence, i.e., solar cycle evolution, in this study, an interesting effect is visible. Namely, in Figure 4, the change of marker color represents the march of time. Red marks show the value of a MS's property around 2010 June and the sequential color variation into blue captures the progress in time. Following the conversion of color from red to blue leads to a trajectory in each figure. In some aspects, at least conceptually, these paths are similar to different branches in the well-known Hertzsprung–Russell diagram (HRD). To characterize these paths in time, the entire problem is simplified to a geometrical problem. Fixed points of these distributions became the geometrical center of "mass," which are marked by a green star in each panel of Figure 4. To give a correct distance of each point from this center point, all the properties are normalized due the different magnitudes of
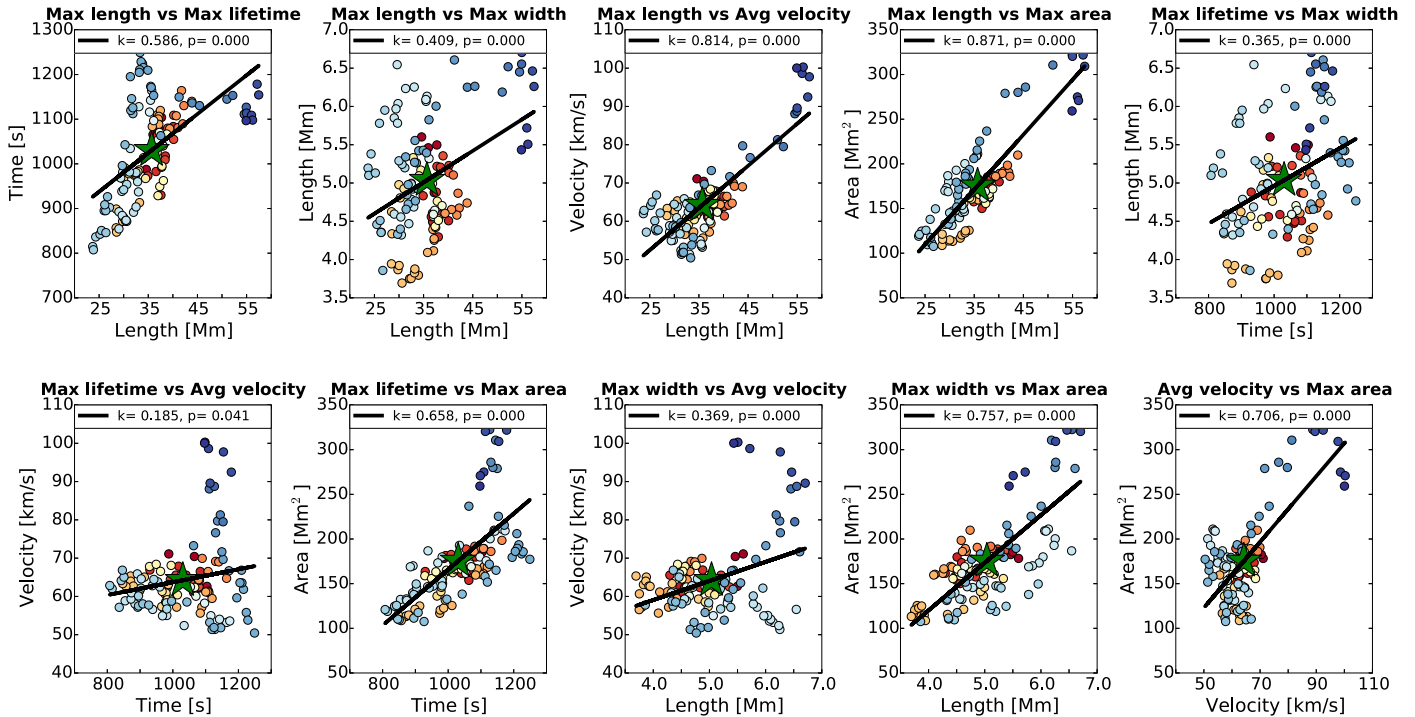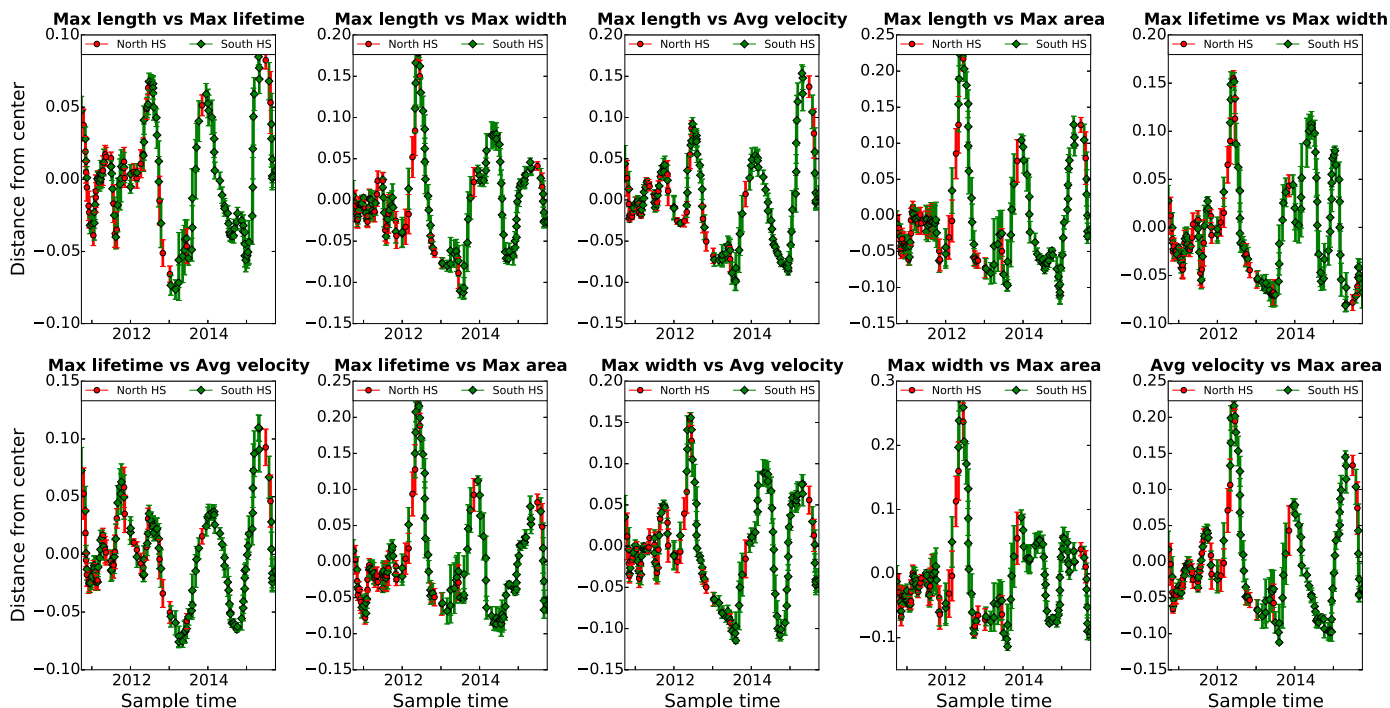
Figure 4. Cross-correlation of a range of MS properties. Variation in color of markers represents the progress in time: red indicates 2010 June, blue indicates 2015 December. A green star indicates the weighted geometric center of property for a given plot. Characteristics of the fitted black line are the *k* correlation coefficient and two-sided *p*-value obtained in a hypothesis test.

values (e.g., lifetime values are three magnitudes greater than maximum width values). After normalization, the geometric distance can be easily worked out. As the cross-correlation distributions suggested, strong temporal variation is visible in

all cases in Figure 5. Multiple strong oscillations are visible in these plots on short timescales ($\tau_{\mathrm{osc}} < 2$ years). Furthermore, the characteristics of the obtained distance curves are different between CH and QS macrospicules, but there is a dominant

Distance from center of mass - Coronal Hole MS

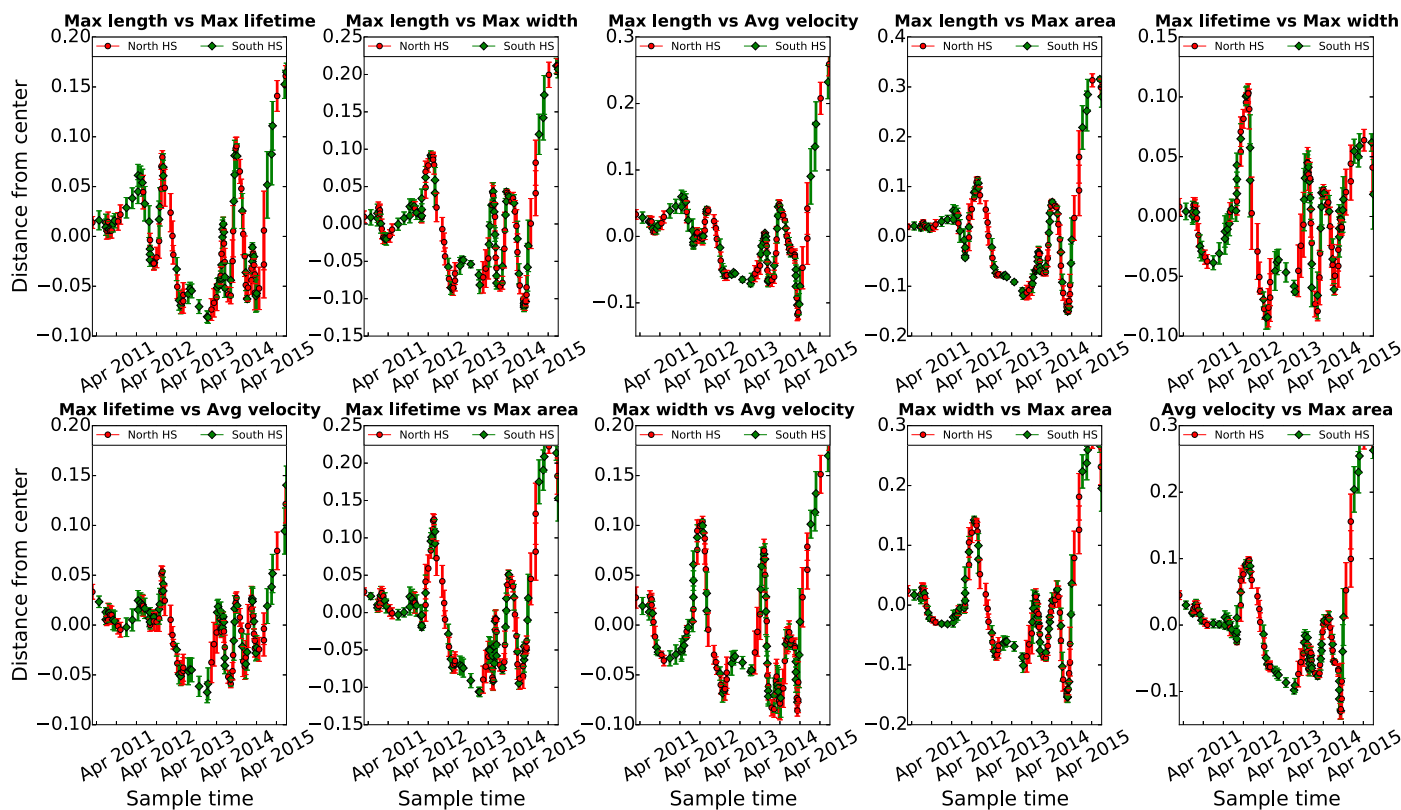

Distance from center of mass - Quiet Sun MS

Figure 5. Distance plot of each mark in Figure 4 from the center of mass. Red points indicates the north hemisphere values, green marks represent MSs from the southern hemisphere.

peak around the first half of 2012 in the majority of the distance plots. All of these suggest that there is a deterministic, underlying, temporal variation in the raw data, which was not known previously, to the best of the authors' knowledge.

Future research of the oscillatory pattern found here may connect macrospicules to oscillatory behavior found in other, large-scale solar phenomena, which have already been reported to show a quasi-biennial oscillation (Fletcher et al. 2010;

Broomhall & Nakariakov 2015) or oscillations with even shorter periods, e.g., found by Cho et al. (2013), Gyenge et al. (2014, 2016).

4. CONCLUSION

The aim of this study is to yield a more accurate and precise statistically relevant characteristic study of the physical properties of macrospicules. For this reason, a data set is built by means of analyzing 301 MSs over a 5.5 year long time interval between 2010 June and 2015 December. The raw data were obtained by *SDO*/AIA using the 30.4 nm wavelength band, where the MS jets were detected at the solar limb. The underlying fundamental principle of this database is to form and apply a range of criteria to MSs that can be summarized into five points. In order to gather information about each MS that fits well the required criteria at every frame of their lifetime, these jets are fitted with tetragons. The diagonals between the edges of the tetragon represent the physical dimensions of the MS, such as length and width.

Five observed properties of MSs were analyzed in this study: maximum length, maximum width, average upflow velocity, maximum area, and lifetime.

Taking advantage of this data set, the spatial distribution of some key parameters of MSs was investigated first. Because ARs were excluded from the solar area of investigation, i.e., where MSs could be identified, the observed jets are found to be at high(er) solar latitudes. CH jets accumulate around the solar poles due to the large-scale open magnetic field of polar CHs. Quiet Sun MSs form a "ring" around them. Further, a strong asymmetry is visible in the number of CH–MSs between the hemispheres. The number of CH–MSs on the southern hemisphere is almost three times larger than that of the northern hemisphere. The source of this difference may be the solar dynamo as has been shown for, e.g., sunspot area (Chowdhury et al. 2013; Kitchatinov & Khlystova 2014). Future research in this topic should seek for a connection between asymmetry indexes of multiple magnetic structures.

Distributions of MS properties in time show a strong temporal variation. To obtain accurate estimates for the average properties, the temporal variation was put aside and their histograms were studied initially. Each histogram was fitted with a log-normal distribution and their preferences (e.g., mode, mean, median, distribution) were determined to characterize the MS. Comparing our findings to those of the previous studies (note that values here are 1σ distribution of the log-normal distributions) we conclude that: lifetime (16.75 ± 4.5 minute), width (6.1 ± 4 Mm), and average velocity (73.14 ± 25.92 km s^{-1}) values are in an agreement, while length (28.05 ± 7.67 Mm) is slightly greater. Agreement between the results found in this research and those in the literature verify the choice of the tetragon assumption.

Last but not least, cross-correlation of the raw data was investigated. When fitting a linear and cross-correlating, there is often a lack of a dominant correlation ($|k_{\mathrm{CH\_avg}}| = 0.372$, $|k_{\mathrm{QS\_avg}}| = 0.57$). In three cases, however, the coefficients are found to be relatively strong for both types of MS. For QS–MSs, two further combinations of physical parameters (i.e., "maximum area versus average velocity" and "maximum area versus maximum lifetime") show a stronger correlation, which may reveal the underlying physical differences between the formation of CH–MSs and QS–MSs. Considering the temporal evolution of these distributions, remarkable paths became visible

in cross-correlation visualizations. To study this behavior, the distances between the center of mass and each point were determined. These distance plots in time reveal a strong, previously unseen, temporal variation in the database.

Broomhall et al. (2009) found that variation of the frequency shift of the global *p*-mode oscillation is a superposition of two oscillators: a stronger one, which has the well-known 11 year long oscillation, and a weaker one, where the period is around two years. These oscillations are named quasi-biennial oscillations (QBOs) and were discovered first by Belmont et al. (1966). QBOs were found in many *global* solar phenomena. Penza et al. (2006) found that the reconstructed data set of the line depth of three photospheric lines over 25 years shows a QBO. Zaqarashvili et al. (2010) investigated the stability of magnetic Rossby waves in the solar tachocline and their results indicate a Rossby wave harmonic with a period of ~2 years, a possible source of QBOs.

Fletcher et al. (2010) suggest that the source of these oscillations could be a second dynamo layer near to the solar surface. Broomhall & Nakariakov (2015) also found QBOs in measuring proxies of the magnetic field in the Sun. Recently, Beaudoin et al. (2016) constructed a double dynamo-layer model that is able to excite QBOs. If *localized* solar features like MSs, by means of statistical investigation of their properties during solar cycle timescales, show a similar behavior, that would suggest a connection between *local* dynamics (e.g., MSs) and the evolution of *global* magnetic field (e.g., solar cycle), an unrevealed question with great potential. Therefore, this will be the focus of our follow-up research.

REFERENCES

Aschwanden, M. 2004, Physics of the Solar Corona (Berlin: Springer)
Beaudoin, P., Simard, C., Cossette, J.-F., & Charbonneau, P. 2016, ApJ, 826, 138
Beckers, J. M. 1968, SoPh, 3, 367
Belmont, A. D., Dartt, D. G., & Ulstad, M. S. 1966, JAtS, 3, 314
Bennett, S. M., & Erdélyi, R. 2015, ApJ, 808, 135
Bohlin, J. D., Vogel, S. N., Purcell, J. D., et al. 1975, ApJ, 197, 133
Broomhall, A.-M., Chaplin, W. J., Elsworth, Y., et al. 2009, ApJ, 700, 162
Broomhall, A.-M., & Nakariakov, V. M. 2015, SoPh, 290, 3095
Chandra, R., Gupta, G. R., Mulay, S., & Tripathi, D. 2015, MNRAS, 446, 3741
Cho, I.-H., Hwang, J., & Park, Y.-D. 2013, SoPh, 289, 707
Chowdhury, P., Choudhary, D. P., & Gosain, S. 2013, ApJ, 768, 188
de Pontieu, B., Carlsson, M., Rouppe, L. H. M., et al. 2012, ApJ, 752, 12
de Pontieu, B., Erdélyi, R., & James, S. P. 2004, Natur, 430, 536
de Pontieu, B., McIntosh, S., Hansteen, V. H., et al. 2007, PASJ, 59, 655
Dere, K. P., Bartoe, J.-D. F., Brueckner, G. E., et al. 1989, SoPh, 119, 55
Erdős, G., & Balogh, A. 2010, JGRA, 115, A01105
Fleck, B., Brekke, P., Haugan, S., Duarte, L., et al. 2000, ESABu, 102, 68
Fletcher, S. T., Broomhall, A.-M., Salabert, D., et al. 2010, ApJL, 718, 19
Gyenge, N., Baranyi, T., & Ludmány, A. 2014, SoPh, 289, 579
Gyenge, N., Bennett, S., & Erdélyi, R. 2015, JApA, 36, 103
Gyenge, N., Ludmány, A., & Baranyi, T. 2016, ApJ, 818, 127
Hoeksema, J. T. SSRv, 72, 137

Judge, P. 2006, in ASP Conf. Ser. 354, Solar MHD Theory and Observations: A High Spatial Resolution Perspective, ed. J. Leibacher, R. F. Stein, & H. Uitenbroek (San Francisco, CA: ASP), 259

Kayshap, P., Banerjee, D., & Srivastava, A. K. 2015, SoPh, 290, 2889

Kayshap, P., Srivastava, A. K., Murawski, K., & Tripathi, D. 2013, ApJ, 770, 3

Kitchatinov, L. L., & Khlystova, A. I. 2014, AstL, 40, 663

Kuridze, D., Henriques, V., Mathioudakis, M., et al. 2015, ApJ, 802, 26

Labonte, B. J. 1979, SoPh, 63, 283

Lee, D., & Deane, A. E. 2009, JCoPh, 228, 952

Lemen, J. R., Title, A. M., Akin, D. J., et al. 2012, SoPh, 275, 17

Lipartito, I., Judge, P. G., Reardon, K., & Cauzzi, G. 2014, ApJ, 785, 109

Madjarska, M., Vanninathan, K., & Doyle, J. G. 2011, A&A, 532, L1

Mumford, S., Pérez-Suárez, D., Christe, S., et al. 2013, in SciPy2013, Proc. 12th Python in Science Conf., ed. S. van der Walt, J. Millman, & K. Huff, 74

Murawski, K., Srivastava, A. K., & Zaqarashvili, T. V. 2011, A&A, 535, A58

Nisticò, G., Zimbardo, G., Patsourakos, S., et al. 2015, A&A, 583, 10

Parenti, S., Bromage, B. J. I., & Bromage, G. E. 2002, A&A, 384, 303

Penza, V., Pietropaolo, E., & Livingston, W. 2006, A&A, 454, 349

Pesnell, W. D., Thompson, B. J., & Chamberlin, P. C. 2012, SoPh, 275, 3

Pike, C. D., & Harrison, R. A. 1997, SoPh, 175, 457

Pike, C. D., & Mason, H. E. 1998, SoPh, 182, 333

Scullion, E., Doyle, J. G., & Erdélyi, R. 2010, MmSAI, 81, 737

Secchi, P. A. 1877, Le Soleil, Vol. 2 (Paris: Gauthier-Villars)

Sekse, D. H., Rouppe, L. H. M., & de Pontieu, B. 2012, ApJ, 752, 108

Shetye, J., Tripathi, D., & Dikpati, M. 2015, ApJ, 799, 220

Sterling, A. C. 2000, SoPh, 196, 79

Sterling, A. C., Harra, L. K., & Moore, R. L. 2010, ApJ, 722, 1644

Sterling, A. C., Moore, R. L., Falconer, D. A., et al. 2015, Natur, 523, 437

Sterling, A. C., Moore, R. L., Falconer, D. A., et al. 2016, ApJ, 821, 100

Vernazza, J. E., Avrett, E. H., & Loeser, R. 1981, ApJS, 45, 635

Zaqarashvili, T. V., Carbonell, M., Oliver, R., & Ballester, J. L. 2010, ApJ, 724, 95

Zaqarashvili, T. V., & Erdélyi, R. 2009, SSRv, 149, 355